Prediction of Long Forcing Waves for Harbor Agitation Studies

Michael Stiassnie[1] and Nitai Drimer[2]

Abstract: An approximate analytical assessment of long wave development due to nonlinear shoaling is obtained and verified against wave-flume experiments. The phase averaged equation for the nonlinear evolution of shoaling waves by Agnon and Sheremet serves as a starting point. Their shoaling interaction function J is significantly simplified through the mild slope assumption. Results, which may be used to assess the long wave input for engineering applications such as harbor resonance studies, are given.

DOI: 10.1061/(ASCE)0733-950X(2006)132:3(166)

CE Database subject headings: Long waves; Random waves; Wave spectra; Harbors; Coastal engineering.

Introduction

For modeling of agitation and berthing conditions in harbors, it is essential to assess the height of long waves near the harbor entrance.

The purpose of this paper is to present an approximate analytical model for the long wave development, to confirm it against new wave flume experiments, and to present practical results for engineering applications.

One manifestation of the quadratic terms in the free-surface boundary condition is the fact that any two waves, with frequencies ω_1 and ω_2, generate two additional waves with frequencies $\omega_1+\omega_2$ and $\omega_1-\omega_2$, called superharmonics and subharmonics, respectively.

The subharmonics for $\omega_1 \approx \omega_2$ have periods significantly larger than those of wind waves, (1 min is a typical value), and are held responsible for the excitation of harbor resonance. Subharmonic waves on water of constant depth are 'bound' to their 'parent' waves, since they propagate with a celerity which is equal to the group velocity of the parent waves. The situation is somewhat different in case of variable water depth. For the latter, Agnon et al. (1993) also show that free subharmonics exist, and derive an appropriate model equation to study the overall evolution for unidirectional cases.

Our knowledge about the incident deep-water wave fields usually comes from wave forecasting models which treat the waves as a stochastic process. In order to calculate the subharmonics, i.e., the long waves, which are generated by stochastic nonlinear shoaling spectra, the Agnon et al. (1993) model was profoundly modified in Agnon and Sheremet (1997). The main results of Agnon and Sheremet (1997) are summarized in the following section.

Next, the shoaling interaction function J is simplified by a stationary phase approach and an analytical solution, which neglects the back influence of the subharmonics on the wind waves, is compared with new laboratory experiments. Finally, guidelines to coastal applications are provided.

Eldeberky and Madsen (1999), as well as Agnon and Sheremet (2000) include surveys of previous relevant references on subharmonics generation.

Basic Equations

Choosing a Cartesian coordinate system (x,y,z), with the y axis at the shoreline, and x,z pointing landward and upward, respectively, the discussion is confined to cylindrical beaches for which the bathymetry is given by $z=-h(x)$, and to wave fields with unidirectional y independent spectra

$$\eta = \mathrm{Re}\sum_f a_f(x)\exp i\left(\int_{-x_0}^{x} k_f(h)dx - \omega_f t + \varepsilon_f\right) \tag{1}$$

where $z=\eta(x,t)$=free-surface elevation and t=time. The wave number k_f is related to the frequency ω_f through the linear dispersion relation

$$\omega_f^2 = g k_f th(k_f h) \tag{2}$$

where g=gravitational acceleration, and $\omega_f=f\omega_0$; $f=1,2,\ldots$. $a_f(x)$=complex amplitudes given as input at say $x=-x_o$, and ε_f=random phase shifts uniformly distributed in $(-\pi,\pi)$.

According to linear water-wave theory

$$|a_f| = (2F_f/Cg_f)^{1/2} \tag{3}$$

F_f=energy flux corresponding to the Fourier mode f, and Cg_f=modal group velocity, given by

[1]Professor, Dept. of Civil and Environmental Engineering, Technion-Israel Institute of Technology, Haifa 32000, Israel (corresponding author). E-mail: miky@tx.technion.ac.il

[2]Director, Coastal And Marine Engineering Research Institute (CAMERI), Technion City, Haifa 32000, Israel. E-mail: nitai@cameri2.technion.ac.il

Note. Discussion open until October 1, 2006. Separate discussions must be submitted for individual papers. To extend the closing date by one month, a written request must be filed with the ASCE Managing Editor. The manuscript for this paper was submitted for review and possible publication on October 1, 2004; approved on August 22, 2005. This paper is part of the ***Journal of Waterway, Port, Coastal, and Ocean Engineering***, Vol. 132, No. 3, May 1, 2006. ©ASCE, ISSN 0733-950X/2006/3-166–171/$25.00.

$$Cg_f = \frac{\omega_f}{2k_f}\left(1 + \frac{2k_f h}{sh(2k_f h)}\right) \tag{4}$$

In the framework of linear theory, the modal energy flux remains constant and is given by

$$F_f = \tfrac{1}{2} Cg_f |a_f(-x_o)|^2 \tag{5}$$

However, Agnon and Sheremet (1997) have shown that due to triad interactions on varying depth the energy fluxes of different modes are interrelated and vary according to

$$\begin{aligned}\frac{dF_f}{dx} = {} & 8\sum_{f_1}\sum_{f_2}[T_{(0,1,2)}F_{f_1}F_{f_2} + T_{(1,-2,0)}F_{f_2}F_f \\ & + T_{(2,-1,0)}F_{f_1}F_f]T_{(0,1,2)}\,\mathrm{Re}\{J_{0:1,2}\}\delta^{\omega}_{0:1,2} \\ & + 16\sum_{f_1}\sum_{f_2}[T_{(0,-1,2)}F_{f_1}F_{f_2} + T_{(1,-0,2)}F_{f_2}F_f \\ & + T_{(2,1,0)}F_{f_1}F_f]T_{(0,-1,2)}\,\mathrm{Re}\{J_{2:0,1}\}\delta^{\omega}_{2:0,1}\end{aligned} \tag{6}$$

while the kernel T is

$$\begin{aligned}T_{(0,\pm1,2)} = {} & \frac{g\omega_f}{8\omega_{f_1}\omega_{f_2}(Cg_f Cg_{f_1}Cg_{f_2})^{1/2}}\Bigg[\pm(2-\Gamma^{\pm})k_{f_1}k_{f_2} \\ & + (1-\Gamma^{\pm})\frac{\omega_{f_1}^2\omega_{f_2}^2}{g^2} + k_{f_1}^2\frac{\omega_{f_2}}{\omega_f} \pm k_{f_2}^2\frac{\omega_{f_1}}{\omega_f} \\ & \mp (1-\Gamma^{\pm})\frac{\omega_f^2\omega_{f_1}\omega_{f_2}}{g^2}\Bigg]\end{aligned} \tag{7}$$

and $\delta^{\omega}_{0:1,2}$=Kronecker delta δ_{f,f_1+f_2}.

The shoaling interaction function J, appearing in Eq. (6), is defined as

$$J_{0:1,2} = \exp\left(-i\int_{-\infty}^{x}\Delta_{0:1,2}dx'\right)\int_{-\infty}^{x}\exp\left(i\int_{-\infty}^{x'}\Delta_{0:1,2}d\xi\right)dx' \tag{8}$$

where $\Delta_{0:1,2}=k_f-k_{f_1}-k_{f_2}$. Note that for the convenience of the reader, the notation as in Agnon and Sheremet (1997) has been followed when possible.

The correction $\Gamma^{\pm}$ in Eq. (7), which was added here to Agnon and Sheremet's (1997) original kernel, and was obtained by Eldeberky and Madsen (1999) is given by

$$\Gamma^{\pm} = 2Cg_f(k_f \mp k_{f_1} - k_{f_2})/\omega_f \tag{9}$$

Mild Slope Assumption

It is assumed that the bottom slope $s=dh/dx$ is small in comparison to the wave-number mismatch $\mu=\Delta_{0:1,2}/k_f$, so that

$$\frac{s}{\mu} = (dh/dx)/(\Delta_{0:1,2}/k_f) = o(1) \tag{10}$$

Integrating the second integral in Eq. (8) twice by parts, and neglecting terms of order s^2/μ^3, when compared to terms of order $1/\mu$ and s/μ^2, gives

$$J_{0:1,2} = -\frac{i}{\Delta^{(-\infty)}_{0:1,2}}\exp\left[-i\int_{-\infty}^{x}\Delta_{0:1,2}\,d\xi\right] - \frac{1}{\Delta^3_{0:1,2}}\frac{d\Delta_{0:1,2}}{dx} - \frac{i}{\Delta_{0:1,2}} \tag{11}$$

Eq. (6) requires two additional integrations [one over x due to the x derivative on its left hand side (l.h.s.), and the other over ω_{f_1} which replaces the Σ_{f_1} on the right hand side (r.h.s.) when ω_0 tends to zero]. Thus, the fast oscillation of the first term in Eq. (11) renders its contribution to the end result much smaller than that of the monotonic terms, and one can replace Eq. (8) by

$$J_{0:1,2} = -\left(\frac{1}{\Delta^3_{0:1,2}}\frac{d\Delta_{0:1,2}}{dx} + \frac{i}{\Delta_{0:1,2}}\right) \tag{12}$$

Nonetheless, Agnon and Sheremet (1997) prove that Eq. (8) is a solution of their Eq. (3.13), which reads

$$\frac{dJ_{0:1,2}}{dx} + i\Delta_{0:1,2}J_{0:1,2} = 1 \tag{13}$$

Substituting Eq. (12) into the l.h.s. of Eq. (13) gives

$$\begin{aligned}\frac{3}{(\Delta_{0:1,2})^4}\left(\frac{d\Delta_{0:1,2}}{dx}\right)^2 - \frac{1}{(\Delta_{0:1,2})^3}\frac{d^2\Delta_{0:1,2}}{dx^2} + \frac{i}{(\Delta_{0:1,2})^2}\frac{d\Delta_{0:1,2}}{dx} \\ - \frac{i}{(\Delta_{0:1,2})^2}\frac{d\Delta_{0:1,2}}{dx} + 1 = 1 + O\left(\frac{s^2}{\mu^2}\right)\end{aligned} \tag{14}$$

which by virtue of Eq. (10) indicates that Eq. (12) is a good approximate solution of Eq. (13), and thus also a good approximation to Eq. (8).

Simplified Solution

Taking an input energy flux at large depth $h_0=h(-x_o)$, for which it is assumed that most of the energy is concentrated in the wind-wave domain

$$F_f|_{x=-x_o} = \begin{cases} F_f^{(h_0)} & \text{for } f = 1,2,\ldots,\hat{f} \quad \text{(long waves)} \\ F_f^{(x_0)} & \text{for } f = \hat{f}+1, \hat{f}+2,\ldots \quad \text{(wind waves)}\end{cases} \tag{15}$$

so that a typical $F_f^{(h_0)}$ is very small compared to the typical $F_f^{(x_o)}$.

Subharmonic waves ($f=1,2,\ldots\hat{f}$) are developed and grow as a result of the nonlinear interaction during the shoaling process. As long as they themselves remain small enough, they do not affect the wind wave significantly, and Eq. (6) simplifies considerably to

$$\frac{dF_f}{dx} = 16\sum_{f_1,f_2}^{f_1,f_2=\hat{f}+1}\sum^{=\infty} T^2_{(0,-1,2)}F^{(x_o)}_{f_1}F^{(x_o)}_{f_2}\,\mathrm{Re}\{J_{2:0,1}\}\delta^{\omega}_{2:0,1}$$

$$\text{for } f = 1,2,\ldots\hat{f} \tag{16}$$

Substituting Eq. (12) into Eq. (16) and integrating gives

$$F_f = F_f^{(h_0)} - 16\sum_{f_1=\hat{f}+1}^{f_1=\infty} F^{(x_o)}_{f_1}F^{(x_o)}_{(f_1+f)}\int_{h_0}^{h} T^2_{(0,-1,0+1)}\frac{\partial\Delta}{\partial h}\frac{dh}{\Delta^3}$$

$$\text{for } f = 1,2,\ldots\hat{f} \tag{17}$$

where

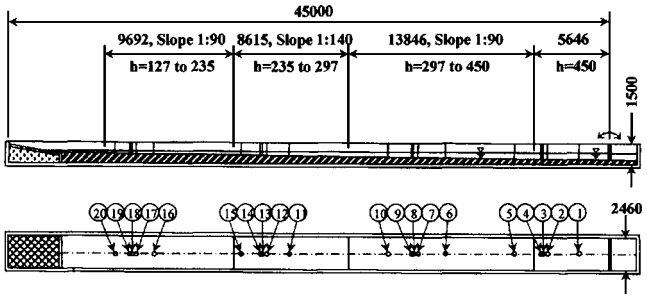

Fig. 1. Wave flume details (all measures are in mm)

$$\Delta = k_{f+f_1} - k_f - k_{f_1} \tag{18}$$

Note that Eq. (17), which is our main result, depends on the local depth h (and not on the coordinate x or the details of the bathymetry) and on the boundary condition at $x=-x_o$, only. The fact that the long waves obtained by the simplified solution Eq. (17) are good approximations to those of the full problem Eq. (6), is demonstrated in the section entitled "Guidelines for Applications."

Comparison with Experiments

Experimental Setup

The experiments were performed in CAMERI's wave flume. The flume is 45 m long (from the wave maker to the end wall), 2.4 m wide, and 1.5 m deep. A rubble mound slope 1:6, 4 m long, covered by a wave-absorbing sheet, is located near the end wall to reduce wave reflection. Fig. 1 presents the experimental setup. The figure indicates flume dimensions, depth, and slope of the sea bed, and location of wave gages.

Twenty wave gages were installed along the centerline of the flume. The use of a set of three wave gages at each measurement station enables decomposition of the recorded wave signal into incident and reflected spectra. The method of decomposition as well as recommendations regarding the distance between the wave gages in a decomposition set are described by Goda (1985). Since the suitable distance is related to the typical wavelength in the spectrum, different triplets to analyze short and long waves were used. The 20 wave gages measure short and long wave spectra at four stations of different depths along the flume (45, 35, 25, and 15 cm deep). At each station, five gages provide a triplet suitable for short wave decomposition and a triplet suitable for long wave decomposition, where the central gage is shared by both triplets. Table 1 indicates the location of the gages, which were sampled at 50 Hz, and the water depth at that location.

For the decomposition of the recorded long waves into incident and reflected parts, it is required to know from theory the wave numbers of the incident and reflected waves related to their period. The long wave energy is distributed between free and

Table 1. Location and Depth of Wave Gages (Central Gauges Are Marked in Bold)

Gauge number	Distance (mm) from wavemaker board	Water depth (mm)
1	2,300	450
2	4,660	450
3	**5,000**	**450**
4	5,100	450
5	7,100	434
6	12,246	377
7	14,346	353
8	**14,646**	**350**
9	14,746	349
10	16,546	329
11	23,945	264
12	25,694	252
13	**25,954**	**250**
14	26,054	249
15	27,554	239
16	34,123	168
17	35,503	152
18	**35,723**	**150**
19	35,823	149
20	37,023	136

Table 2. Input Data for Pierson–Moskowitz Spectra at $h=45$ cm

Experiment number	*H*short (cm)	*Tp* spectral peak (s)	*H*long (cm)
PM-1	1.43	0.74	0.02
PM-2	2.23	0.78	0.03
PM-3	2.88	1.17	0.05
PM-4	4.20	1.26	0.14
PM-5	5.15	1.26	0.25

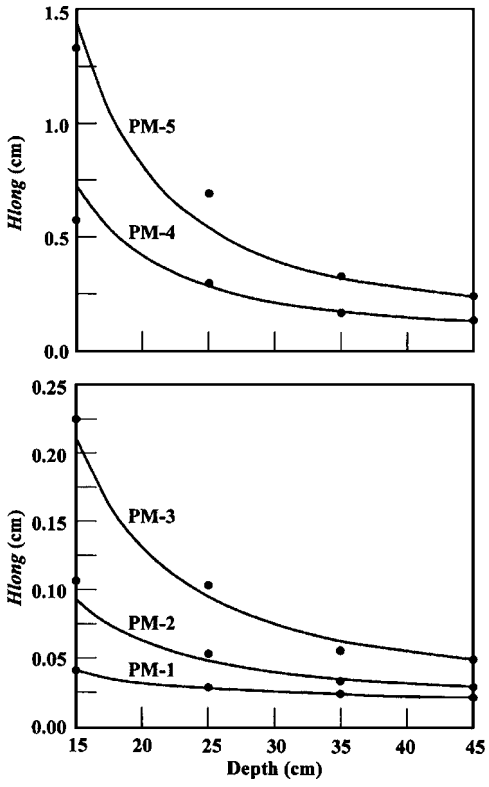

Fig. 2. Comparison of theoretical results with experiments

Table 3. Nondimensional Characteristic Height of Long Waves $\hat{H}$long As Function of Nondimensional Depth $\hat{h}$ for Different Peak Enhancement Factors γ

$\hat{h}$	$\gamma=1$	$\gamma=2.8$	$\gamma=4$	$\gamma=7$
6.00	0.0001	0.0001	0.0001	0.0001
5.00	0.0142	0.0143	0.0144	0.0144
4.00	0.0246	0.0250	0.0252	0.0253
3.00	0.0410	0.0425	0.0431	0.0436
2.50	0.0543	0.0569	0.0578	0.0588
2.00	0.0768	0.0814	0.0830	0.0848
1.80	0.0899	0.0956	0.0975	0.0998
1.60	0.1074	0.1145	0.1169	0.1196
1.40	0.1318	0.1406	0.1436	0.1470
1.20	0.1674	0.1787	0.1825	0.1868
1.00	0.2237	0.2388	0.2438	0.2493
0.90	0.2640	0.2818	0.2877	0.2942
0.80	0.3193	0.3409	0.3480	0.3558
0.75	0.3545	0.3786	0.3866	0.3953
0.70	0.3974	0.4246	0.4335	0.4434
0.65	0.4503	0.4814	0.4916	0.5029
0.60	0.5169	0.5532	0.5650	0.5781
0.55	0.6029	0.6458	0.6598	0.6754
0.50	0.7168	0.7688	0.7858	0.8047
0.45	0.8729	0.9377	0.9587	1.9822
0.40	1.0957	1.1790	1.2060	1.2363
0.35	1.4306	1.5422	1.5783	1.6190
0.32	1.7125	1.8482	1.8920	1.9414
0.30	1.9521	2.1083	2.1587	2.2156
0.28	2.2509	2.4328	2.4914	2.5577
0.26	2.6297	2.8443	2.9134	2.9917
0.24	3.1193	3.3764	3.4591	3.5529
0.22	3.7669	4.0802	4.1810	4.2954
0.20	4.6467	5.0367	5.1621	5.3045
0.18	5.8819	6.3799	6.5398	6.7218
0.16	7.6875	8.3436	8.5542	8.7940
0.14	10.4649	11.3649	11.6536	11.9825
0.12	15.0320	16.3337	16.7509	17.2267
0.10	23.2558	25.2823	25.9313	26.6719

locked waves, which have different dispersion relations. Hence, two different approaches were utilized. In the first approach, the long incident and long reflected waves were assumed to behave as free waves and have their wave number given by the linear dispersion relation Eq. (2). In the second approach, the reflected long waves were assumed to behave as free waves, whereas the incident long waves were assumed to be bound waves with celerities equal to the group velocity of the spectral peak of the short waves. The incident wave heights produced by the above decompositions were within 15% from each other.

The difference in the heights of the reflected waves obtained by the two different decomposition approaches was significant, but their energy content in shallow water was small in comparison to the energy of the incident waves.

The values for *H*long incident *H*long reflected for all experiments, and for both decomposition approaches, are given in Tables 5 and 6 in the Appendix. In the sequel the results from the first approach, which assumes free long waves, are adopted.

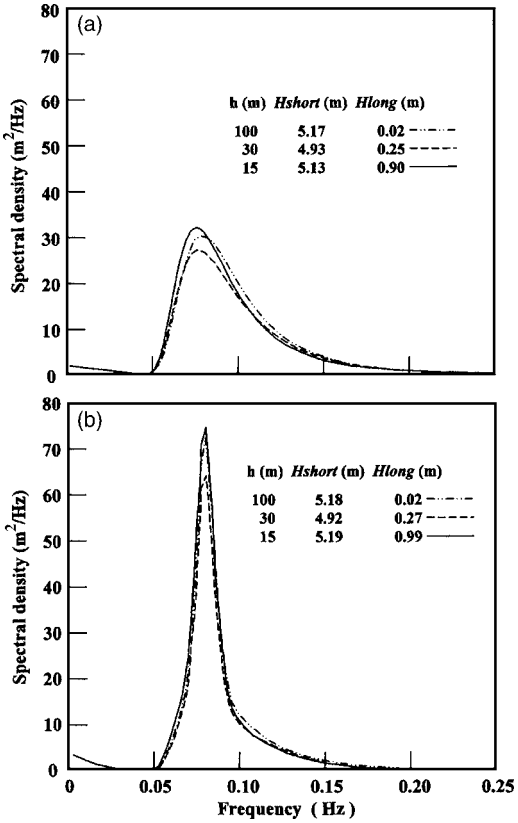

Fig. 3. Evolution of JOWSWAP spectra with depth. Deep water conditions are: *H*short=5.2 m and T_p=12.6 s: (a) $\gamma=1$ and (b) $\gamma=4$.

Input Parameters

The wave generation signal was obtained by applying an inverse discrete Fourier transform on the Pierson–Moskowitz spectrum. For each experiment, the duration of generation signal was 900 s.

However, the real input parameters taken as boundary conditions for comparison of theory and experiments are those of the incident spectrum as measured at the deepest station (45 cm). The input parameters are given in Table 2.

In Table 2 and elsewhere, *H*short is the total characteristic wave height (H_{mo}), defined as four times the square root of the area under the spectral density function

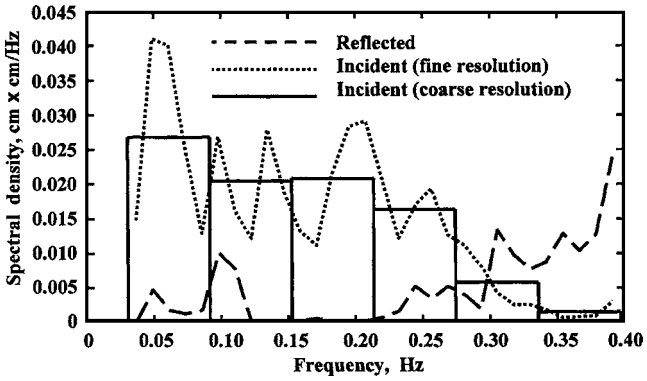

Fig. 4. Spectral density of long waves for experiment PM-4 at water depth of 25 cm

Table 4. Long Waves at $h=6$ m: Comparison of Simplified and Exact Solutions for JONSWAP Spectra with $\gamma=2.8$

T_p (s)	9.4	9.4	10.9	12.9	12.2	12.2	13.4	13.4	14.4	14.4
Hshort (m)	2	2.3	1.6	2	1.5	2.2	1.3	1.6	1.5	1.9
Hlong (m) from Eq. (6)	0.50	0.67	0.41	0.67	0.45	0.98	0.45	0.70	0.71	1.09
Hlong (m) from Table 3	0.49	0.65	0.45	0.70	0.51	1.09	0.43	0.65	0.71	1.14

$$H\text{short} = 4\left(\frac{1}{2}\sum_{f\geq\hat{f}+1} a_f^2\right)^{1/2} \tag{19}$$

Hlong=characteristic wave height of the long waves, i.e., those with frequencies smaller than $\omega_0\left(\frac{1}{2}+\hat{f}\right)\approx 0.40$ Hz

$$H\text{long} = 4\left(\frac{1}{2}\sum_{f=1}^{\hat{f}} a_f^2\right)^{1/2} \tag{20}$$

In the present study, $\hat{f}=6$.

Although the wave generation signal does not include long wave energy, it was generated in the flume due to reflection.

For comparison with theory each input spectrum was represented by 41 bins, of which the first six were considered as long waves (periods above 2.5 s). The first bin had the frequency $\omega_0=0.06104$ Hz, which is also the frequency difference between bins. Each bin contained five frequencies of the measured input spectrum.

Results

Fig. 2 gives the theoretical and measured characteristic long wave height as function of water depth. The continuous curves present the theoretical solution given by Eq. (17), while the experimental results are given at the four depths of measurement. The largest depth (45 cm) is the input depth. The theory assesses the evolution of long wave energy from a given (deep) water depth toward the shallow water. Due to wave reflection, the experimental results present considerable long wave energy at the deep water near the wave generator. In Fig. 2 the input wave spectrum for each theoretical run is the measured one at water depth of 45 cm, including the long wave energy.

The experiment reference name, as given in Table 2 for the input parameters, is indicated near each curve.

The characteristic height of the long waves Hlong, depends on the choice of the frequency that distinguishes between short and long waves. This frequency is not rigorously defined; however, it should be selected in the interval of low energy density, which usually exists between the ranges of short and long waves in spectral energy plots. The frequency distinction of 0.4 Hz was selected in view of the spectral energy distribution obtained in the measurements. Obviously, when theoretical and experimental results are compared, the same frequency of distinction is selected.

The agreement between the calculated and measured results for all cases is rather satisfactory.

The distribution of energy in the long wave range for broad spectra is discussed in the following section. Generally speaking, the comparison between the experiments and theory indicates the usefulness of the latter for practical applications, which are addressed in the following section.

Guidelines for Applications

The simplified solution Eq. (17) enables us to provide data which can serve as guidelines for field applications in a rather condensed fashion. Starting in deep water with $F_f^{(h_0)}\equiv 0$ and $F_f^{(x_0)}$ as determined from JONSWAP spectra with different peak enhancement factors γ, one can use Eq. (17) to obtain Table 3 for the nondimensional long wave characteristic wave height

$$\hat{H}\text{long} = gT_p^2 H\text{long}/4\pi^2 H\text{short}^2 \tag{21}$$

where Hshort=characteristic height of the Joint North Sea Wave Project (JONSWAP) spectrum in deep water, and T_p=its peak period.

The nondimensional depth in the left column of Table 3 is

$$\hat{h} = 4\pi^2 h/gT_p^2 \tag{22}$$

In the construction of Table 3, long waves were defined as those with wave periods larger than twice the spectral peak period. From the table, one can see that narrow spectra (i.e., large γ) produce somewhat larger long waves than broad spectra.

To demonstrate the use of Table 3, consider the case Hshort=5.2 m; $T_p=12.6$ s; $\gamma=4$; and $h=15$ m. For this case Eq. (22) gives $\hat{h}=0.38$, and the table yields $\hat{H}$long=1.4, and finally from Eq. (21) Hlong=0.95 m.

Some caution should be taken when using Table 3 for applications. Namely, one should not use the table whenever $H\text{short} > h/2$, since wave breaking is expected; and when Hlong turns out to be larger than 0.3 Hshort, for which the assumption of the simplified solution starts to lose its validity.

For harbor resonance studies, one needs Hlong as well as information about the spectral distribution of the long waves energy. From the calculated examples in Fig. 3 one can see that the long waves spectral density can be roughly approximated by a linear decrease, from a maximum at frequency $\rightarrow 0$ to zero at frequency $\approx$ half the peak frequency. The quasitriangular shape of the spectral density of the long waves is also evident from the experiments, as one can see in Fig. 4. Fig. 4 gives the spectral density of the long waves for experiment PM-4 at a water depth of 25 cm. It includes the measured incident and reflected parts of

Table 5. Analyzed Incident/Reflected Long Waves from Experiments (in cm) for Free Incident Waves

	Depth (cm)			
Experiment	45	35	25	15
PM-l	0.02/0.01	0.03/0.01	0.03/0.01	0.04/0.03
PM-2	0.03/0.02	0.04/0.02	0.05/0.03	0.11/0.11
PM-3	0.05/0.04	0.06/0.04	0.10/0.06	0.23/0.13
PM-4	0.14/0.13	0.17/0.12	0.30/0.17	0.58/0.28
PM-5	0.25/0.18	0.33/0.17	0.69/0.29	1.33/0.43

Table 6. Analyzed Incident/Reflected Long Waves from Experiments (in cm) for Locked Incident Waves

	Depth (cm)			
Experiment	45	35	25	15
PM-1	0.02/0.02	0.02/0.02	0.03/0.03	0.04/0.03
PM-2	0.03/0.02	0.03/0.03	0.07/0.05	0.12/0.08
PM-3	0.06/0.04	0.07/0.04	0.12/0.04	0.24/0.08
PM-4	0.15/0.10	0.19/0.11	0.33/0.11	0.61/0.16
PM-5	0.28/0.20	0.33/0.20	0.72/0.21	1.35/0.49

the spectrum. The bar diagram in Fig. 4 gives the incident spectral density in a coarse frequency resolution, which is the same as the one that has been used in solving Eq. (17).

To strengthen confidence in the values provided by Table 3, they have been checked against results obtained by solving Eq. (6) directly (see Sheremet and Stiassnie 1996). The input in this comparison consists of JONSWAP spectra with $\gamma=2.8$, and various combinations of Hshort and T_p. In Table 4 values of Hlong, for water depth $h=6$ m, as calculated from Table 3 and as computed from Eq. (6) are compared, and found to agree within 10%.

Note that another possible mechanism for the generation of long waves is related to the breaking of wave groups and to the surf zone (see Baldock et al. 2004). However, Battjes et al. (2004) claim that on mild slopes this breakpoint generation is ineffective compared to subharmonic generation which dominates. In any case, harbor entrances are usually well outside the surf zone.

Acknowledgments

The present work emerged from a study that M.S. began in the summer of 1996, while visiting the International Research Center for Computational Hydrodynamics (ICCH) in Denmark. He is grateful to Professor Per A. Madsen and the staff at ICCH for their hospitality. Many fruitful discussions with Professor Yehuda Agnon are much appreciated.

Appendix

The results of the first approach, for which free incident long waves and free reflected long waves are assumed, are presented in Table 5.

The results of the second approach, for which locked incident long waves and free reflected long waves are assumed, are presented in Table 6.

References

Agnon, Y., and Sheremet, A. (1997). "Stochastic nonlinear shoaling of directional spectra." *J. Fluid Mech.*, 345, 79–99.

Agnon, Y., and Sheremet, A. (2000). "Stochastic evolution models for nonlinear gravity waves over uneven topography." *Advances in coastal and ocean engineering*, P.L.-F. Liu, ed., Vol. 6, World Scientific, Singapore, 103–131.

Agnon, Y., Sheremet, A., Gonsalves, J., and Stiassnie, M. (1993). "Nonlinear evolution of a unidirectional shoaling wave field." *Coastal Eng.*, 20, 29–58.

Baldock, T. E., O'Hare, T. J., and Huntley, D. A. (2004). "Long wave forcing on a barred beach." *J. Fluid Mech.*, 503, 321–343.

Battjes, J. A., Bakkenes, H. J., Janssen, H. J., and Van Dongeren, A. R. (2004). "Shoaling of subharmonic gravity waves." *J. Geophys. Res.*, 109(C2), CO 2009, 1–15.

Eldeberky, Y., and Madsen, P. A. (1999). "Deterministic and stochastic evolution equations for fully dispersive and weakly nonlinear waves." *Coastal Eng.*, 38, 1–24.

Goda, Y. (1985). *Random seas and design of maritime structures*, University of Tokyo Press, Tokyo.

Sheremet, A., and Stiassnie, M. (1996). "Laboratory validation of nonlinear shoaling computations." *ICZM in the Mediterranean & Black Sea, Proc., Int. Workshop*, Sarigerme, Turkey, 391–403.